ISSN 1560-0904, Polymer Science, Ser. B, 2014, Vol. 56, No. 6, pp. 909–918. © Pleiades Publishing, Ltd., 2014.

Spherical Mesoporous Silica Nanoparticles/Tailor-Made Polystyrene Nanocomposites by In Situ Reverse Atom Transfer Radical Polymerization[1]

Khezrollah Khezri[a], Hossein Roghani-Mamaqani[b], Mohammadreza Sarsabili[c], Masoud Sobani[d], and Seyed-Ataollah Mirshafiei-Langari[d]

[a] *School of Chemistry, University College of Science, University of Tehran, P.O. Box 14155-6455, Tehran, Iran*
[b] *Department of Polymer Engineering, Sahand University of Technology, P.O. Box 51335-1996, Tabriz, Iran*
[c] *Department of Chemical Engineering, Gas, and Petroleum, Semnan University, PO Box: 35131-19111, Semnan, Iran*
[d] *Department of Polymer Engineering and Color Technology, Amirkabir University of Technology, P.O. Box 15875-4413, Tehran, Iran*
e-mail: kh.khezri@ut.ac.ir

Received June 2, 2014;
Revised Manuscript Received August 12, 2014

Abstract—Spherical mesoporous silica nanoparticles (MCM-41)/tailor-made polystyrene nanocomposites were synthesized by in situ reverse atom transfer radical polymerization. Characteristics of spherical MCM-41 nanoparticles were evaluated by nitrogen adsorption/desorption isotherm and X-ray diffraction. Morphological studies were also performed by scanning and transmission electron microscopy. Conversion and molecular weight evaluations were carried out using gas and size exclusion chromatography respectively. Addition 3 wt% of MCM-41 nanoparticles results in a decrease in conversion from 89 to 53%. Similar reduction behavior is also observed for molecular weight of the nanocomposites. However, polydispersity indices (PDI) values increase from 1.42 to 2.07 by the only 3 wt% addition of MCM-41 nanoparticles. A peak around 4.1 ppm which originates from hydrogen atom of terminal units of polymer chains in ^{1}H NMR spectra in combination with low PDI values can appropriately demonstrate the living nature of the polymerization. Thermogravimetric analysis shows that thermal stability of the nanocomposites is higher than the neat polystyrene and increases by increasing MCM-41 nanoparticles content. Glass transition temperature decreases by the addition of MCM-41 nanoparticles loading as revealed by differential scanning calorimetry results.

DOI: 10.1134/S1560090414660026

INTRODUCTION

Polymer nanocomposites have attracted much attention because weak polymer matrices can be reinforced by addition of inorganic nanofillers such as layered silicates, silica nanoparticles, metal oxides (e.g. Fe_3O_4, TiO_2 and ZnO) [1–7]. Addition of small amounts of inorganic nanofillers in an organic polymer matrix, results in significant improvements in thermal stability and flame retardancy [8], mechanical strength [9], gas permeation [10], modulus [11] and some other properties of the neat polymer. Polymer nanocomposites combine the advantages of both polymers (e.g. flexibility, ductility, and processability) and inorganic nanofillers (e.g. rigidity and thermal stability) [12, 13]. Although usage of inorganic nanoparticles in a polymer matrix provides many benefits, nanoparticles aggregation and the lake of strong interaction between the polymer matrix and nanofillers are two important problems which can restrict wide applications of these nanofillers. Therefore, synthesis of appropriate polymer nancomposites depends significantly on homogeneous distribution of inorganic nanoparticles in polymer matrices. Without reduction of surface energy and therefore agglomeration of nanofillers, homogeneous distribution in the polymer matrix can not be achieved [14–16]. Main properties of polymer nanocomposites are generally affected by both of the nature of polymer matrices and nanofiller characteristics. Moreover, they can be influenced by processing conditions. Physical mixing and polymerization in the presence of inorganic nanofillers are two main methods for preparation of polymer nanocomposites [14, 15].

The first report on M41S family materials can be dated back to 1992 in which the Mobil Oil Company was discovered the first mesoporous silica material. Unlike the Zeolit, M41S have pore diameters approximately from 2 to 10 nm. This property in combination with very large surface area, ordered pore systems, and well-defined pore radius distributions make this family as unique nanomaterials [17, 18]. M41S family has been classified into four main groups: disordered rods

[1] The article is published in the original.

and three others are well defined structures which are MCM-41, MCM-48 with a three-dimensional cubic pore structure and MCM-50 with an unstable lamellar structure [19]. MCM-41 as a popular member of M41S family possesses a porous system consisting of hexagonally arranged channels with diameters of 15 to 100 Å. MCM-41 is more attended due to its high specific surface area, high thermal and hydrothermal stability, possibility of controlling its pore size, its hydrophobicity, and acidity [20, 21]. These unique merits have made MCM-41 as a promising material in several research areas such as nanoscience, polymer composites, environmental purification, catalyst, ion exchange systems, chromatography, and drug delivery [22–24].

Free radical polymerization (FRP) is one of the most common industrial synthetic methods to prepare numerous polymeric materials. FRP can be applied to large families of monomers, polymerization systems and various polymerization media and therefore it is a popular procedure for industrial processes. Despite its abundant advantages, synthesis of well-defined architectures, such as block copolymers, star polymers, and hyperbranched structures, is not possible by FRP. Also, lack of control over the molecular weight and polydispersity of polymer chains is another deficiency of FRP. Therefore, development of various controlled radical polymerization (CRP) techniques has opened an appropriate way to synthesize of polymer chains with predetermined molecular weight, well-defined structures, and low polydispersity indices (PDI) [26–28]. Among the three most common CRP methods, nitroxide-mediated polymerization (NMP), reversible addition fragmentation chain transfer (RAFT), and atom transfer radical polymerization (ATRP), ATRP presents several benefits over the others. Applicability to a wide variety of monomers and polymerization systems, commercial availability of its reactants, and also application of different initiation technique are some advantages of the ATRP systems. Additionally, dynamic equilibrium between the dormant species and propagating radicals can be easily adjusted for an ATRP system by modifying complexing ligand of the catalyst [27, 29].

Review of related literature indicates that application of CRP techniques has been largely considered for the preparation of favorite mesoporous silica nanoparticles/polymer nanocomposite. Preparation of interesting core-shell nanostructure with mesoporous silica nanoparticles and polymer around the exterior surface of the nanoparticles via surface RAFT polymerization has reported by Hong et al. [30–31]. Bals et al. employed surface-initiated NMP for grafting polystyrene chains in both the inner and outer surface of mesoporous silica nanoparticles. They applied various types of mesoporous silica nanoparticles with different morphologies and pore sizes [32]. Pasetto et al. produced hybrid materials by grafting poly(methyl methacrylate) and polystyrene chains on the surface of mesoporous silica nanoparticles via surface-initiated ATRP (SI–ATRP) [33]. They used various types of mesoporous silica nanoparticles like micrometric particles, submicrometric polydisperse spherical particles, and monodisperse core-shell particles as substrates. They evaluated the macromolecular features of free and attached polymer chains. Also, core-shell nanostructure with mesoporous silica nanoparticles core and hyperbranched poly(2-((bromobutyryl)oxy)ethyl acrylate) shell has reported by Li et al. via surface-initiated self condensing ATRP. According to their results, hybrid nanoparticles were dispersed appropriately in the organic solvents [34]. Meer et al. investigated the effect of mesoporosity on the thermal and mechanical properties of silica/polystyrene nanocomposites [14]. In their study, mesoporous and colloidal silica nanoparticles were incorporated into polystyrene matrices via two different methods of melt blending and SI–ATRP. Their results indicate that both of the nanocomposites have grafted polymer with similar characteristics.

In this study, advantages of reverse atom transfer radical polymerization (RATRP) were applied to the synthesis of tailor-made polystyrene matrices. Initial reagents of RATRP are less sensitive to oxygen and can be easily prepared and therefore synthetic procedure can be facilitated. Moreover, by RATRP, oxidation problems of normal ATRP can be circumvented. Incorporation of MCM-41 nanoparticles into the polystyrene matrix was performed by in situ polymerization method. Synthesis and characterization of MCM-41 nanoparticles, investigating the effect of MCM-41 nanoparticles on RATRP and thermal properties of the nanocomposites are discussed.

EXPERIMENTAL

Materials

Styrene (Aldrich, 99%) was passed through an alumina-filled column to remove inhibitors. Copper(II) bromide ($CuBr_2$, Fluka, 99%), *N*,*N*,*N*',*N*'',*N*''-pentamethyldiethylenetriamine (PMDETA, Aldrich, 99%), 2,2'-azobisisobutyronitrile (AIBN, Acros), anisole (Aldrich, 99%), tetrahydrofuran (THF, Merck, 99%), neutral aluminum oxide (Aldrich, 99%), ammonium solution (Merck, 25 wt% in water), ethanol (Merck, 99%), cetyltrimethylammonium bromide (CTAB, Merck, 97%), and tetraethoxysilane (TEOS, Merck) were used as received.

Synthesis of Spherical Mesoporous Silica Nanoparticle

At first, CTAB (5.01 g, 13.7 mmol) was dissolved in 100 mL of deionized water and vigorously stirred for 5 min until the solution became clear. Then, 37.4 mL of ammonium solution was slowly added to the CTAB solution under stirring to form gel like mixture. Then, the solution was left under stirring for 10 min. Afterward, ethanol (152 mL) was added to the solution and

stirred 20 min. Subsequently, TEOS (10.2 mL, 0.03 mmol) was added dropwise during 30 min and left under stirring for 3 h. The white powder was precipitated, filtered, and washed with deionized water several times and then dried in vacuum oven at 110°C for 48 hours. To remove CTAB, the white powder was calcinated at 550°C for 6 hours with the heating rate of 10°C/min.

Polymerization of Styrene via RATRP

Reverse atom transfer radical polymerization of styrene was performed in a 100 mL three-neck lab reactor, which equipped with a reflux condenser, nitrogen inlet valve, and a magnetic stir bar that was placed in an oil bath. A typical batch of polymerization was run at 110°C with the molar ratio of 100 : 1 : 1 : 1 for [Styrene] : [$CuBr_2$] : [AIBN] : [PMDETA] giving a theoretical polymer molecular weight of 10423 g/mol at final conversion. Styrene (15 mL), $CuBr_2$ (0.399 g, 1.74 mmol), PMDETA (0.36 mL, 1.74 mmol) and anisole (7 mL) were transferred to reactor and the reactor was degassed and back-filled with nitrogen gas three times, and then left under N_2 and stirring was continued. The solution turned green color as the $CuBr_2$/PMDETA complex was formed. When the majority of the metal complex had formed, reaction temperature was increased to 110°C during 5 min. Subsequently, AIBN (0.286 g, 1.74 mmol) as a monomer soluble radical initiator (dissolved in 5 mL styrene) was injected into the reactor to start the polymerization. In the case of nanocomposites, a desired amount of MCM-41 nanoparticles was suspended in 10 mL styrene and it was agitated for 15 h. Then, the polymerization procedure was applied.

Designation of the samples with the amounts of MCM-41 nanoparticles is given in Table 1. PPS refers to pure polystyrene and PSC X implies different nanocomposites of polystyrene with various amounts of MCM-41 nanoparticles.

Separation of Polymer Chains from MCM-41 Nanoparticles and Catalyst Removal

For separating polymer chains from MCM-41 nanoparticles, nanocomposites were dissolved in THF. By high-speed ultracentrifugation (10000 rpm) and then passing the solution through a 0.2 micrometer filter, polymer chains were separated from MCM-41 nanoparticles. Subsequently, polymer solutions passed through an alumina column to remove catalyst.

Characterization

X-ray diffraction spectra were collected on an X-ray diffraction instrument (Siemens D5000) with a Cu target ($\lambda = 0.1540$ nm). The system consists of a rotating anode generator operated at 35 kV and 20 mA current. The samples were scanned from $2\theta = 2°$ to 10° at the step scan mode, and the diffraction pattern was recorded using a scintillation counter detector. The basal spacing or d_{001}-spacing of the samples were calculated using Bragg's law of diffraction ($\lambda = 2d\sin\theta$). Materials porosity was characterized by N_2 adsorption/desorption curves obtained with a Quntasurb QS18 (Quntachrom) apparatus. The surface area and pore size distribution values were obtained with the corrected BET equation and Broekhoff and de Boer-models, respectively. A Vega Tescan SEM analyzer (Czech Republic) was used to evaluate surface morphology of the powder samples which were gold-coated using a sputtering coater. The specimens were prepared by coating a thin layer on a mica surface using a spin coater (Modern Technology Development Institute, Iran). Also, transmission electron microscope (TEM), FEG Philips CM, with an accelerating voltage of 200 kV was used. Gas chromatography (GC) is a simple and highly sensitive characterization method and does not require removal of the metal catalyst particles. GC was performed on an Agilent-6890N with a split/splitless injector and flame ionization detector, using a 60 m HP-INNOWAX capillary column for the separation. The GC temperature profile included an initial steady heating at 60°C for 10 min and a 10 grad/min ramp from 60 to 160°C. The samples were also diluted with acetone. The ratio of monomer to anisole was measured by GC to calculate monomer conversion throughout the reaction. Size exclusion Chromatography (SEC) was used to measure the molecular weight and molecular weight distribution. A Waters 2000 ALLIANCE with a set of three columns of pore sizes of 10000, 1000, and 500 Å was utilized to determine polymer average molecular weight and polydispersity index (PDI). THF was used as the eluent at a flow rate of 1.0 mL/min, and calibration was carried out using low polydispersity polystyrene standards. Proton nuclear magnetic resonance spectroscopy (^{1}H NMR) spectra were recorded on a Bruker 300-MHz ^{1}H NMR instrument with $CDCl_3$ as the solvent and tetramethylsilane as the internal standard. Thermal gravimetric analysis (TGA) was carried out with a PL thermo-gravimetric analyzer (Polymer Laboratories, TGA 1000, UK). Thermograms were obtained from ambient temperature to 700°C at a heating rate of 10 grad/min. Thermal analysis were

Table 1. Designation of the samples

Sample	Preparation method	Proportion of MCM-41, wt %	Time of MCM-41 dispersion, h
PPS	RATRP	0	–
PSC 1	In situ RATRP	1	15
PSC 2	In situ RATRP	2	15
PSC 3	In situ RATRP	3	15

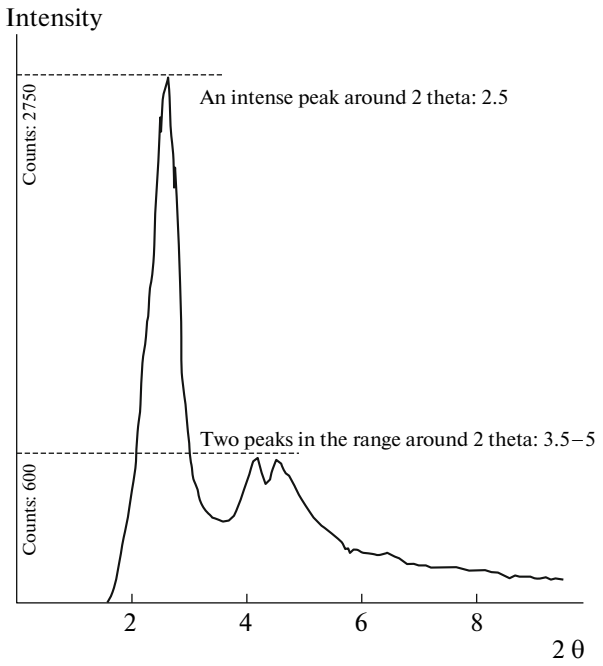

Fig. 1. XRD graph of the MCM-41 nanoparticles.

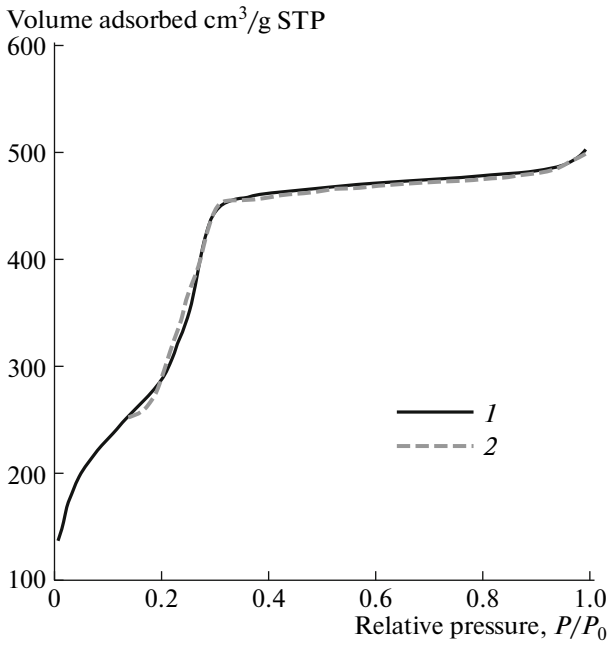

Fig. 2. Nitrogen (*1*) absorption/(*2*) desorption isotherm of MCM-41 nanoparticles.

carried out using a differential scanning calorimetry (DSC) instrument (NETZSCH DSC 200 F3, Netzsch Co, Selb/Bavaria, Germany). Nitrogen at a rate of 50 mL/min was used as purging gas. Aluminum pans containing 2–3 mg of the samples were sealed using DSC sample press. The samples were heated from ambient temperature to 220°C at a heating rate of 10°C/min.

RESULTS AND DISCUSSION

Characteristics and morphology of MCM-41 nanoparticles is an important factor which affects the properties of nanocomposites. Specific structure of the MCM-41 nanoparticles was determined by XRD. A sharp and intense peak around $2\theta = 2.5°$ and also some weak peaks in the diffraction angles of about $2\theta = 3–5°$ can be attributed to the well-hexagonal structure of the MCM-41 nanoparticles [22, 35] (Fig. 1).

Nitrogen adsorption/desorption isotherm of the calcined MCM-41 nanoparticles is shown in Fig. 2. During nitrogen physisorption experiment, the synthesized sample reveals mesoporous materials behavior and shows IV isotherm according to the International Union of Pure and Applied Chemistry (IUPAC) classification. The isotherm can be divided into three sections: 1—a linear increase in nitrogen adsorption which takes place at low relative pressure due to monolayer adsorption of N_2 on the wall of MCM-41 nanoparticles, 2—Capillary condensation of nitrogen inside the mesopores (narrow pore size distribution can be indicated), 3—a long plateau at higher pressures due to the low adsorption of N_2 on the external surface of calcined MCM-41 nanoparticles (saturation step) [22, 35]. Extracted data from this analysis is summarized in Table 2.

SEM has employed to examine morphology, size and size distribution of MCM-41 nanoparticles. According to the SEM images, MCM-41 nanoparticles are spherical. Although the particles size is mainly in the range of 500 to 800 nm, some larger particles are also observed (around 1000 nm). By suspending of dried powder in water, an interesting image was captured. Porosity of spherical nanoparticle is clearly displayed in Fig. 3b.

Porosity of structure and pore condition of the MCM-41 nanoparticles was evaluated by TEM. Figure 4 depicts TEM images of pristine MCM-41 naoparticles in two different magnifications. According to

Table 2. Extracted data from nitrogen adsorption/desorption isotherm of the calcined MCM-41 nanoparticles

BET surface area, m^2/g	Langmuir surface area, m^2/g	Average pore diameter (4V/A by BET), Å	BJH adsorption average pore diameter (4V/A), Å	BJH desorption average pore diameter (4V/A), Å
1068.13	1496.31	28.72	25.49	24.97

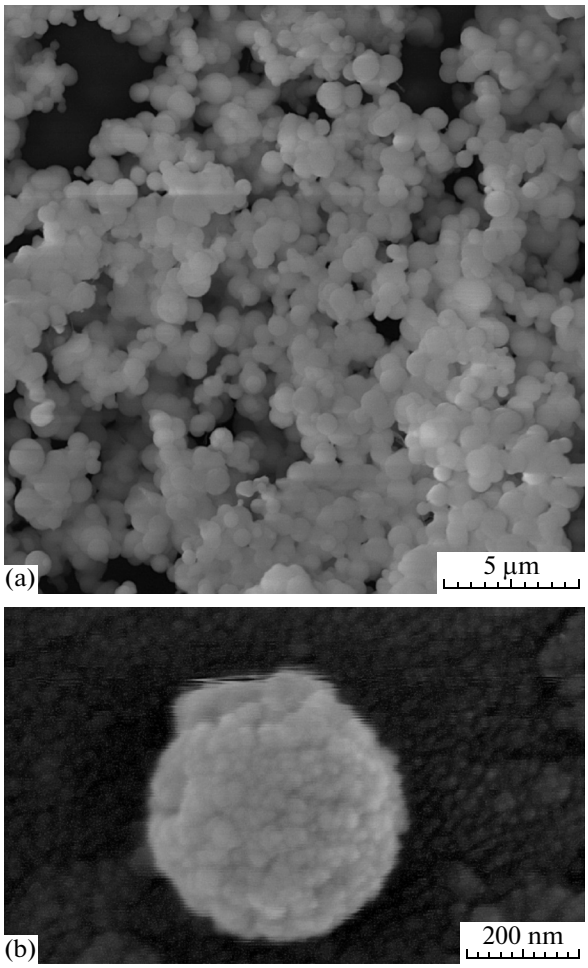

Fig. 3. SEM images of the MCM-41 nanoparticles: (a) powder and (b) suspended in water.

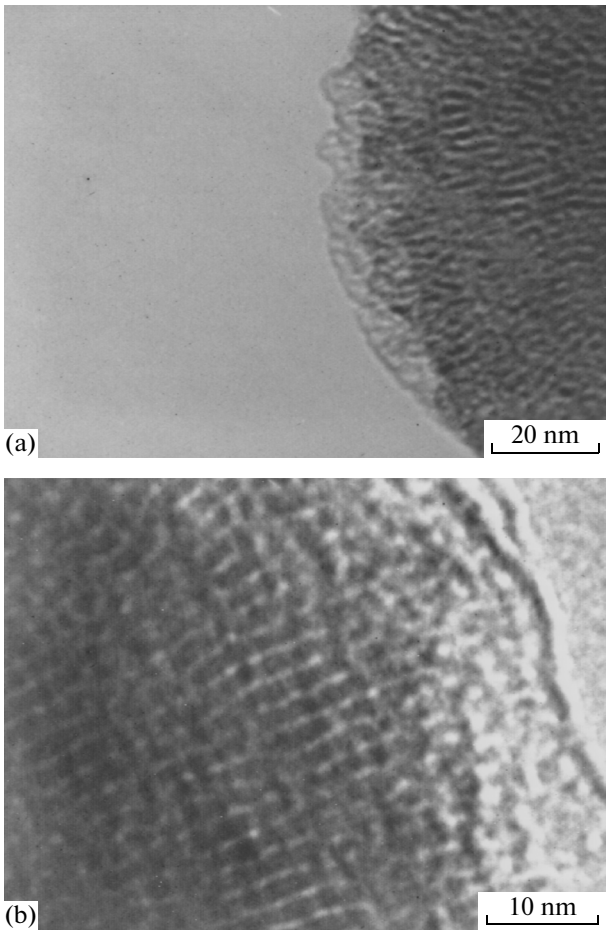

Fig. 4. TEM images of the synthesized MCM-41 nanoparticles in two different magnifications.

these images, porous structure with regular hexagonal channels of the synthesized MCM-41 naoparticles can be clearly demonstrated.

The possibility of ATRP to employ various initiation techniques is a unique feature of this polymerization method. Although normal ATRP is an advantage route to synthesize tailor-made polymers, it suffers from oxidation of catalyst by air. Therefore, RATRP is developed to circumvent this deficiency. The reactants of RATRP are less sensitive to oxygen and can be easily prepared and therefore synthetic procedure can be facilitated [10, 36, 37]. General procedure for preparation of MCM-41/tailor-made polystyrene nanocomposites is shown in Fig. 5.

Evaluation of molecular weight and PDI values of the extracted polymers and the effect of MCM-41 nanoparticles addition are carried out by SEC. As illustrated in Fig. 6, SEC traces of the neat polystyrene and all the nanocomposites are monomodal. Wide distribution of molecular weights is mainly attributed to the nature of radical initiator and initiation process. Generally, AIBN-induced living radical polymerization always results in polymers with high PDI value when the molar ratio of the deactivator to that of the initiating radicals is equal to the unity. According to the fact that in the initiation step of RATRP (AIBN : $CuBr_2$: PMDETA), a reversible equilibrium between growing radicals and dormant species can be quickly established after the induction periods. Thus, concentrations of the active species or propagating radicals will be maintained sufficiently low which leads to narrow PDI values. However, in the last step of the polymerization, insufficient deactivation of the propagating radicals can result in higher PDI values (final PDI values are reported in this study) [10, 36, 38]. Therefore, lower PDI values and narrow molecular weight distribution can be achieved by using higher amount of deactivator.

Increasing MCM-41 nanoparticles content in the polystyrene matrix, results in considerable effects on the conversion, molecular weights, and PDI values (Table 3). Broadening of SEC traces by adding MCM-41 nanoparticles indicates that these nanoparticles as a filler influences the equilibrium of ATRP reaction. MCM-41 nanoparticles as an impurity can increase chain transfer and termination reactions of propagat-

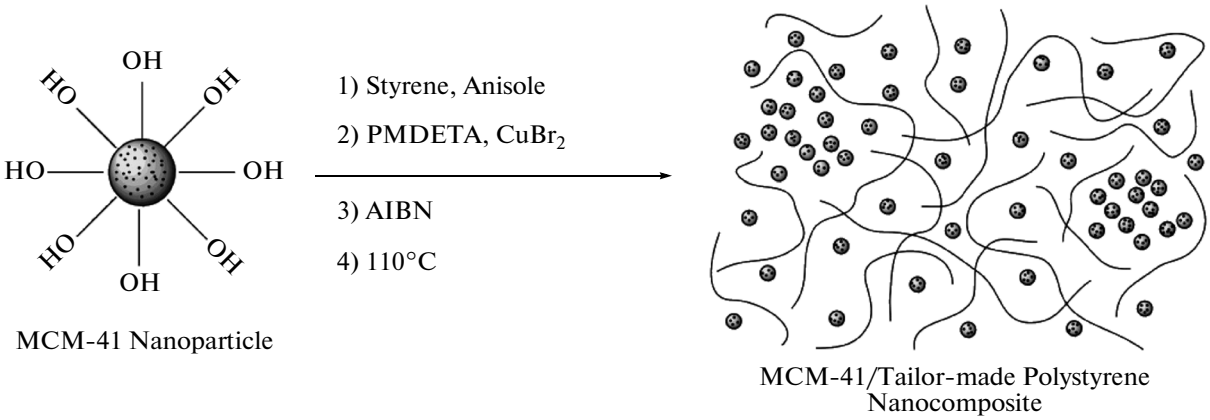

Fig. 5. General procedure for the synthesis of MCM-41 nanoparticles/polystyrene nanocomposites.

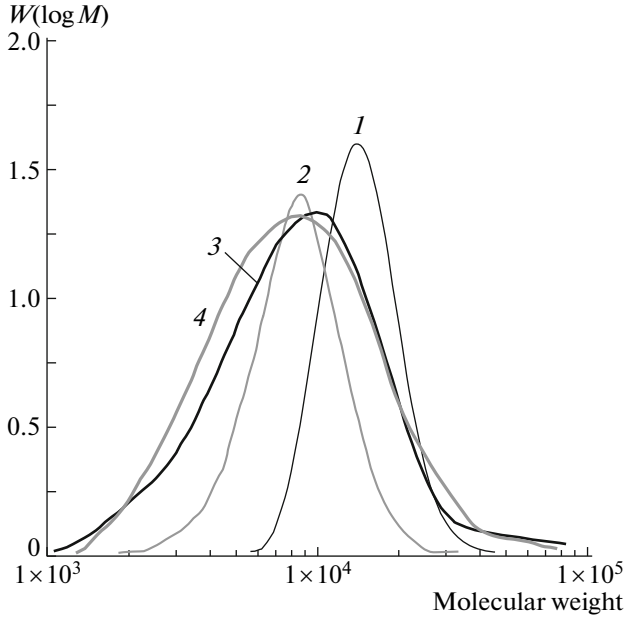

Fig. 6. SEC trace of (*1*) the neat polystyrene PPC, and its nanocomposites (*2*) PSC 1, (*3*) PSC 2, (*4*) PSC 3.

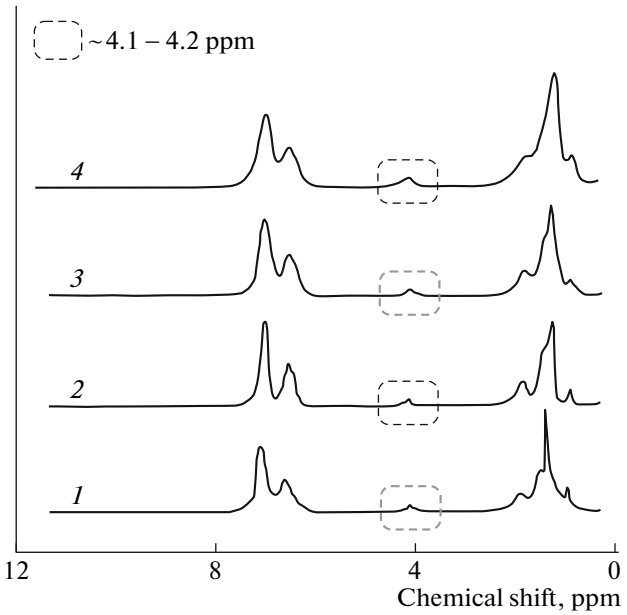

Fig. 7. ^{1}H NMR spectra of (*1*) the neat polystyrene PPC, and its nanocomposites (*2*) PSC 1, (*3*) PSC 2, (*4*) PSC 3.

ing radicals, and therefore broadens molecular weight distribution of the resultant polymers [39, 40]. Color change of reaction media during polymerization (from light green to light brown) is convenient evidence of ATRP equilibrium establishment [10, 41, 42]. Increasing PDI values from 1.41 to 2.07 and decreasing of molecular weights and also conversion depends on the nature of MCM-41 nanoparticles. High concentration of hydroxyl groups on the surface of MCM-41 nanoparticles displays a key role. An irreversible reaction between growing radicals and functional moieties on the surface of MCM-41 nanoparticles confirms the results. Therefore, the chance of growing radicals to participate in irreversible reactions will be increased by increasing MCM-41 nanoparticles content [11, 43]. Moreover, mobility of macroradicals in the solution can be restricted by MCM-41 nanoparticles (particularly at higher loading) and therefore polymerization rate and conversion decrease by incrementing of MCM-41 nanoparticles loading [44].

Evaluation of polymer chain composition can be investigated by ^{1}H NMR spectroscopy. ^{1}H NMR spectra of the neat polystyrene and its nanocomposites are presented in Fig. 7. The marked peak around 4.1–4.2 ppm, which originates from hydrogen atom of terminal units of polymer chains (–CHBr), provides an appropriate evidence for living feature of polymerization. Moreover, inherent peaks of polystyrene chains such as benzene rings, methylene ($-CH_2-$), and tertiary carbon hydrogen [$-CH(C_6H_5)-$] appears in the spectra at the vicinity of about 7.40–6.25, 1.71–1.15, and 2.31–1.71 ppm, respectively [9].

Table 3. Molecular weights and PDI values of the extracted polystyrene chains resulted from SEC traces

Sample	Reaction time, h	Conversion, %	M_n, g/mol		M_w, g/mol	PDI
			Exp.	Theo.		
PPS	6	89	11137	9276	15814	1.42
PSC 1	6	77	7218	8026	12343	1.71
PSC 2	6	68	5964	7088	11272	1.89
PSC 3	6	53	5036	5524	10425	2.07

Thermal stability of the neat polystyrene and its nanocomposites is evaluated by TGA. TGA thermograms of the weigh loss as a function of temperature in the temperature window of 30–700°C in addition to their corresponding differential thermogravimetric curves (DTG) are presented in Fig. 8.

Noticeable improvement in thermal stability of the nanocomposites in comparison with the neat polystyrene is presented in Figure 8. Thermal stabilities of all the nanocomposites are higher than the neat polystyrene and it increases by increasing the MCM-41 nanoparticles content. Three separate steps of degradation can be seen in the Fig. 8: 1—Desorption of chemisorbed water and the silanol groups on the surface of MCM-41 nanoparticles in which all the adsorbed water on the pure MCM-41 nanoparticles is removed at about 100°C [45, 46]. 2—Degradation of volatile materials such as residual monomer, MCM-41 functionalities, and low molecular weight oligomers. 3—The main degradation step which relates to the synthesized polymers and nanocomposites. Char values of the samples at 600°C are presented in Table 4. Char values increases by increasing MCM-41 nanoparticles content. Also, MCM-41 nanoparticles leaves 96.32% char after complete degradation at 600°C. In Fig. 9, degradation temperature of the samples against amount of degradation is plotted to prove the fact that by adding MCM-41 nanoparticles content in the polymer matrix, thermal stability improves (T_X: temperature threshold at which X% of the polystyrene and its nanocomposites degradation is occurred).

Improving thermal stability of the nanocomposites by increasing MCM-41 nanoparticles loading can be attributed to the high thermal stability of MCM-41 nanoparticles and also interaction between MCM-41 nanoparticles and polystyrene matrix [47]. Physical interaction between polystyrene chains and surface of the MCM-41 nanoparticles and finally degradation from outer surface inward can be considered as important factors for increasing thermal stability of the nanocomposites [14]. Table 4 summarized the extracted data from TGA (char values) and DTG curves which indicates an improvement in thermal stability of the nanocomposites by increasing MCM-41 nanoparticles content.

Glass transition temperature (T_g) and the effect of nanoparticles on chain confinement are evaluated by DSC. Figure 10 presents DSC thermograms of the neat polystyrene and its nanocomposites with different MCM-41 nanoparticles content. Since MCM-41

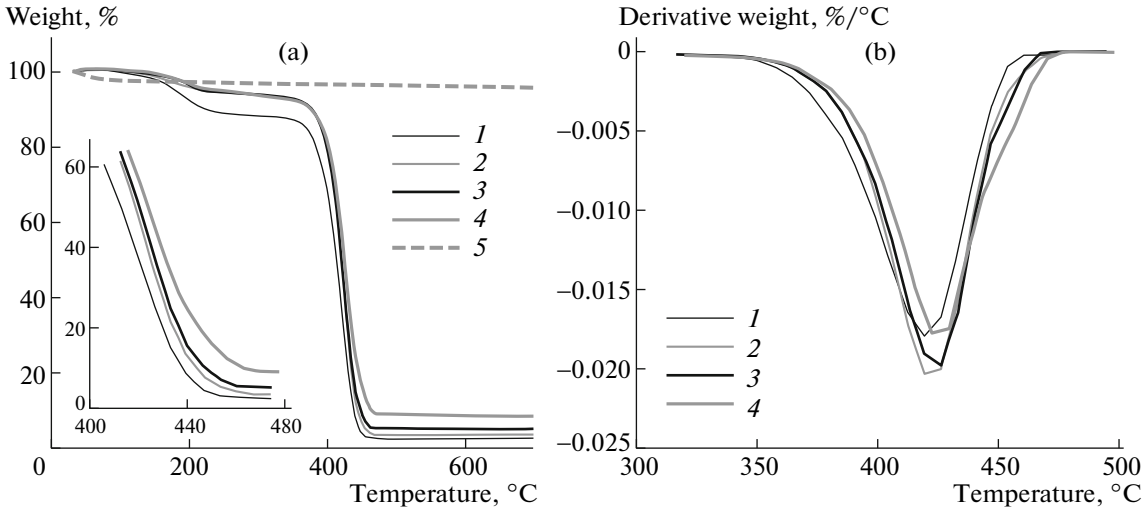

Fig. 8. (a) TGA and (b) DTG thermograms of (*1*) the neat polystyrene PPC, and its nanocomposites (*2*) PSC 1, (*3*) PSC 2, (*4*) PSC 3, and (*5*) MCM-41.

Table 4. Extracted data from TGA and DTG for the neat polystyrene and its nanocomposites

Sample	TGA	DTG, °C		
	Char, % at 600°C	Start point	Peak point	End point
PPS	2.60	352	419	457
PSC 1	3.59	360	422	470
PSC 2	5.09	360	423	470
PSC 3	8.61	361	424	471

Table 5. Extracted T_g of the neat polystyrene and its nanocomposites

Sample	M_n, g/mol	PDI	T_g, °C
PPS	11137	1.42	100.9
PSC 1	7218	1.71	95.8
PSC 2	5964	1.89	92.9
PSC 3	5036	2.07	91.5

nanoparticles do not bear any transitions in this range of temperature, therefore only thermal transition of polystyrene is observed. In these experiments, samples were heated from room temperature to 220°C. Then, they were cooled to room temperature for distinguishing the phase conversion and other irreversible thermal behaviors. Finally, the samples were heated from room temperature to 220°C to evaluate T_g values.

As it can be seen in the Fig. 10, an obvious inflection in the heating path is occurred which shows T_g of the samples. Corresponding inflection in the cooling path is also appeared and it is necessary to mention that there is not another peak in this path which indicates that the structure of synthesized polystyrene and its nanocomposites are mainly amorphous and they have not gone through crystallization phenomenon. Extracted T_g from DSC graphs are presented in Table 5.

According to these results, T_g value of the neat polystyrene is higher than all of the nanocomposites and by increasing of MCM-41 nanoparticles content, a decrease in T_g value takes place which may be attributed to the weak interaction between polystyrene chains and hydroxyl groups of MCM-41 nanoparticles. Thus, MCM-41 nanoparticles can reduce the packing polystyrene chains and therefore increase the segments mobilities which in turn results in T_g reduction. Moreover, other parameters such as decrease in molecular weights and increment of PDI values need to be considered since decrease of molecular weight results in decrease of T_g and high PDI values may cause reduction of T_g values. This is mainly on account of the fact that in very high PDI values, chains with low molecular weights can act as viscosity reducer like plactisizers. In addition, homogeneous dispersion of MCM-41 nanoparticles is restricted because of strong tendency of MCM-41 nanoparticles to agglomerate

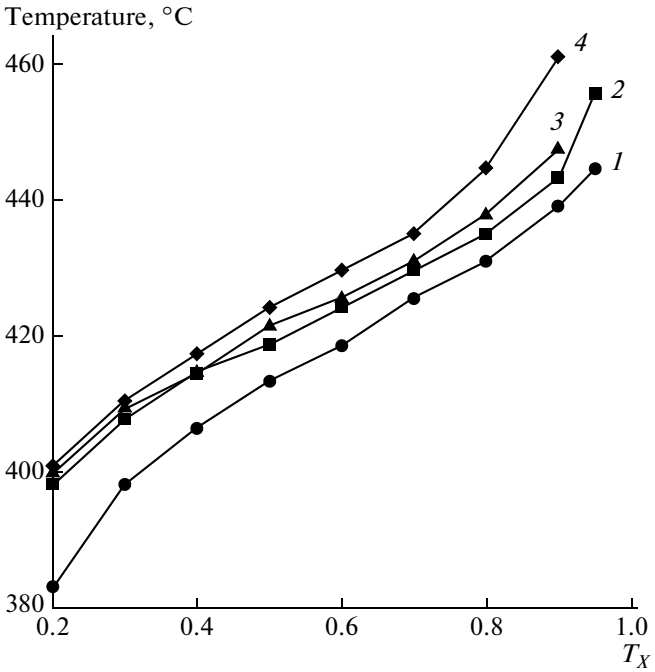

Fig. 9. Graphical illustration temperature and degradation relationship of (*1*) the neat polystyrene PPC, and its nanocomposites (*2*) PSC 1, (*3*) PSC 2, (*4*) PSC 3.

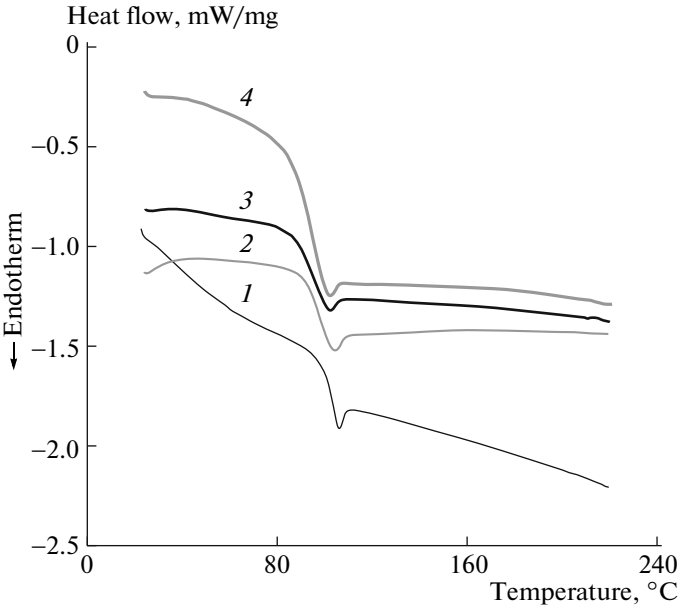

Fig. 10. DSC thermogram for (*1*) the neat polystyrene PPC, and its nanocomposites (*2*) PSC 1, (*3*) PSC 2, (*4*) PSC 3.

(to reduce their surface energy). Therefore, some free volume spaces for the dangling polystyrene chains within matrices may be created as a resultant of MCM-41 nanoparticles aggregation which results in decrement of T_g values. Numerous studies have demonstrated that the glass transition temperature of polymers can be changed upon addition of low content of nanoparticles [48, 49]. In this context, reduction of T_g values by increasing nanoparticles into the polymer matrix are plenty reported. Schadler et al. have demonstrated that by addition very low content of alumina nanoparticles, a considerable decrement of T_g was occurred (however at high loadings, further reduction was not observed) [50]. Sarsabili et al. have also reported that the synthesized nanocomposites via FRP, have lower T_g values in comparison with neat polystyrene [44]. Moreover, in the case of silica aerogel nanoparticles, in general, the prepared nanocomposite show lower T_g values than neat polystyrene [51].

CONCLUSIONS

In situ RATRP was successfully applied to synthesize tailor-made polystyrene matrices with random dispersion of MCM-41 nanoparticles. Spherical morphology, well-hexagonal structure and high surface area with small and regular pore diameters are demonstrated for the synthesized MCM-41 nanoparticles. Considerable decrease in conversion from 89 to 53% and from 11137 to 5036 g/mol for number molecular weight were occurred by 3 wt% addition of MCM-41 nanoparticles. Moreover, PDI values were also increased from 1.42 to 2.07. Low intensity peak in the vicinity of around 4.1 ppm in ^{1}H NMR spectra in combination with the SEC-extracted data demonstrate the living nature of polymerization. By addition of 3 wt% MCM-41 nanoparticles, thermal stability of the nanocomposites increases and T_g values decreases from 100.9 to 91.5°C.

REFERENCES

1. Q. T. Nguyen and D. G. Baird, Adv. Polym. Technol. **25**, 270 (2006).
2. K. Khezri, V. Haddadi-Asl, H. Roghani-Mamaqani, and M. Salami-Kalajahi, J. Appl. Polym. Sci. **124**, 2278 (2012).
3. Q. Sun, Y. Deng, and Z. L. Wang, Macromol. Mater. Eng. **289**, 288 (2004).
4. G. Al-Ghamdi, E. D. Sudol, V. L. Dimonie, and M. S. El-Aasser, J. Appl. Polym. Sci. **101**, 3479 (2006).
5. G. Qiu, Q. Wang, C. Wang, W. Lau, and Y. Guo, Polym. Int. **55**, 265 (2006).
6. K. Khezri and H. Roghani-Mamaqani, Mater. Res. Bull. **59**, 241 (2014).
7. E. Tang and S. Dong, Colloid Polym. Sci. **287**, 1025 (2009).
8. B. N. Jang, M. Costache, and C. A. Wilkie, Polymer **46**, 10678 (2005).
9. A. Fujimori, N. Ninomiya, and T. Masuko, Polym. Adv. Technol. **19**, 1735 (2008).
10. S. Nazarenko, P. Meneghetti, P. Julmon, B. Olson, and S. Qutubuddin, J. Polym. Sci., Part B: Polym. Phys. **45**, 1733 (2007).
11. D. Shia, C. Y. Hui, S. D. Burnside, and E. P. Giannelis, Polym. Compos. **19**, 608 (1998).
12. L.-P. Wang, L.-M. Zhao, and W.-Z. Li, React. Funct. Polym. **70**, 35 (2010).
13. L. Wei, N. Hu, and Y. Zhang, Materials **3**, 4066 (2010).
14. M. A. V. Meer, B. Narasimhan, B. H. Shanks, and S. K. Mallapragada, ACS Appl. Mater. Interfaces **2**, 41 (2010).
15. R. Rovira-Truitt, N. Patil, F. Castillo, and J. L. White, Macromolecules **42**, 7772 (2009).
16. R. Rotzoll, D. H. Nguyen, and P. Vana, Macromol. Symp. **275–276**, 1 (2009).
17. X. Liu, H. Sun, Y. Chen, Y. Yang, and A. Borgna, Microporous Mesoporous Mater. **121**, 73 (2009).
18. A. Stein, B. J. Melde, and R. C. Schroden, Adv. Mater. **12**, 1403 (2000).
19. S. Bhattacharyya, G. Lelong, and M.-L. Saboungi, J. Exp. Nanosci. **1**, 375 (2006).
20. R. A. A. Melo, M. V. Giotto, J. Rocha, and E. A. Urquieta-González, Mater. Res. **2**, 173 (1999).
21. H.-P. Lin, S. Cheng, and C.-Y. Mou, Chem. Mater. **10**, 581 (1998).
22. M. Teymouri, A. Samadi-Maybodi, and A. Vahid, Int. Nano Lett. **1**, 34 (2011).
23. T. Yasmin and K. Müller, J. Chromatogr. A **1217**, 3362 (2010).
24. L. Huang, H. Xiao, and Y. Ni, Colloids Surf., A **247**, 129 (2004).
25. C.-Y. Mou, and H.-P. Lin, Pure Appl. Chem. **72**, 137 (2000).
26. D. Chikhaoui-Grioune, A. Aqil, A. M. Zalfen, A. Benaboura, and C. Jérome, J. Appl. Polym. Sci. **117**, 1005 (2010).
27. W. Braunecker and K. Matyjaszewski, Prog. Polym. Sci. **32**, 93 (2007).
28. J. Qiu, B. Charleux, and K. Matyjaszewski, Prog. Polym. Sci. **26**, 2083 (2001).
29. P. B. Zetterlund, Y. Kagawa, and M. Okubo, Chem. Rev. **108**, 3747 (2008).
30. C.-Y. Hong, X. Li, and C.-Y. Pan, Eur. Polym. J. **43**, 4114 (2007).
31. C.-Y. Hong, X. Li, and C.-Y. Pan, J. Phys. Chem. C **112**, 15320 (2008).
32. H. Blas, M. Save, C. Boissiere, C. Sanchez, and B. Charleux, Macromolecules **44**, 2577 (2011).
33. P. Pasetto, H. Blas, F. Audouin, C. Boissiere, C. Sanchez, M. Save, and B. Charleux, Macromolecules **42**, 5983 (2009).
34. X. Li, C.-Y. Hong, and C.-Y. Pan, Polymer **51**, 92 (2010).
35. X. M. Tai, H. X. Wang, and X. Q. Shi, Chin. Chem. Lett. **16**, 843 (2005).
36. Z. Cheng, X. Zhu, L. Zhang, N. Zhou, J. Chen, and J. Macromol. Sci., Part A: Pure Appl. Chem. 40, 371 (2003).

37. K. Khezri, V. Haddadi-Asl, and H. Roghani-Mamaqani, NANO **9**, 1450023 (2014).
38. K.-Y. Qiu and P. Li, Chin. J. Polym. Sci. **22**, 99 (2004).
39. K. Khezri and H. Roghani-Mamaqani, J. Compos. Mater. (2014), DOI: 10.1177/0021998314535961
40. M. Sobani, V. Haddadi-Asl, M. Salami-Kalajahi, H. Roghani-Mamaqani, S.-A. Mirshafiei-Langari, and K. Khezri, J. Sol-Gel Sci. Technol. **66**, 337 (2013).
41. K. Khezri, V. Haddadi-Asl, H. Roghani-Mamaqani, and M. Salami-Kalajahi, J. Polym. Res. **19**, 9868 (2012).
42. K. Matyjaszewski, J. Qiu, N. Tsarevsky, and B. Charleux, J. Polym. Sci., Part A: Polym. Chem. **38**, 4724 (2000).
43. S. A. Bon and P. J. Colver, Langmuir **23**, 8316 (2007).
44. M. Sarsabili, M. Parvini, M. Salami-Kalajahi, and A. Asfadeh, Iran. Polym. J. **22**, 155 (2013).
45. Z. Liu, Z. Dong, B. Han, J. Zhang, J. Zhang, Z. Hou, J. He, and T. Jiang, J. Mater. Chem. **13**, 1373 (2003).
46. L. D. Pérez, J. F. López, V. H. Orozco, T. Kyu, and B. L. López, J. Appl. Polym. Sci. **111**, 2229 (2009).
47. S. Subramania, S. W. Choia, J. Y. Lee, and J. H. Kim, Polymer **48**, 4691 (2007).
48. F. Chen, A. Clough, B. M. Reinhard, M. W. Grinstaff, N. Jiang, T. Koga, and O. K. C. Tsui, Macromolecules **46**, 4663 (2013).
49. B. Natarajan, Y. Li, H. Deng, L.C. Brinson, and L. S. Schadler, Macromolecules **46**, 2833 (2013).
50. B. J. Ash, R. W. Siegel, and L. S. Schadler, J. Polym. Sci., Part B: Polym. Phys. **42**, 4371 (2004).
51. S.-A. Mirshafiei-Langari, V. haddadi-Asl, H. Roghani-Mamaqani, M. Sobani, and K. Khezri, J. Polym. Res. **20**, 163 (2013).